Future (2015-2100) Antarctic-wide ice-shelf firn air depletion from a statistical firn emulator

Devon Dunmire[1*], Nander Wever[1,2], Alison F. Banwell[3], Jan T.M. Lenaerts[1]

[1] Department of Atmospheric and Oceanic Sciences, University of Colorado, Boulder, CO, USA

[2] WSL Institute for Snow and Avalanche Research SLF, Davos, Switzerland

[3] Cooperative Institute for Research in Environmental Sciences (CIRES), University of Colorado, Boulder, CO, USA

[*] Corresponding author. Email: devon.dunmire@colorado.edu

This preprint is in the first round of revisions at *Nature Communications Earth & Environment*.

Abstract

Antarctic firn is critical for ice-shelf stability because it stores meltwater that would otherwise pond on the surface. Ponded meltwater increases the risk of hydrofracture, and subsequent potential ice-shelf collapse. Here, we use output from a firn model to build a computationally simpler emulator that uses a random forest to predict ice-shelf firn air content (FAC) based on climate conditions. We find that summer air temperature and precipitation are the most important climatic features for predicting FAC. By 2100, Larsen C Ice Shelf is most at risk of firn air depletion, while the larger Ross and Ronne-Filchner are likely to experience little FAC change. Variability in Earth System Model projections is the largest uncertainty source regarding future FAC predictions. In fact, the model uncertainty, described by the firn air depletion spread from CMIP6 models in the SSP3-7.0 and SSP5-8.5 emission scenarios, is larger than the firn air depletion range across the emission scenarios.

Keywords: Antarctica, ice shelves, firn modelling, firn depletion

1 Introduction

Since 1979, Antarctic Ice Sheet (AIS) mass loss has contributed to 14.0 ± 2.0 mm of global mean sea-level rise[1]. This mass loss occurs primarily via increased ice discharge, as ice flows faster from the interior of the ice sheet into floating ice shelves, which surround 75% of the continent[2] and regulate the ocean-ward flow of inland ice[3,4]. As ice shelves weaken and thin, their buttressing effect reduces, allowing inland ice to flow faster, which contributes more to global sea-level rise[5,6].

Two important processes have been identified as key to future ice-shelf thinning, weakening and retreat: i) ocean-warming-induced basal melting[7,8], and ii) atmospheric-warming-induced surface melting[9–11]. The latter may result in ponded surface meltwater, which can lead to hydrofracture, whereby the hydrostatic pressure of ponded meltwater propagates fractures through the entire ice-shelf thickness. Hydrofracture has been implicated in the break-up of several Antarctic ice shelves including the 2002 near-complete disintegration of Larsen B[12–14] and the 2008 partial break-up of Wilkins[15]. These processes are a major source of uncertainty for assessing future sea level rise from increased land ice flow, given the limited quantitative understanding of ice-shelf instability processes and ice shelf-land ice interactions[16].

Currently, most Antarctic meltwater percolates into and refreezes within the porous firn layer. However, if meltwater repeatedly refreezes without sufficient firn replenishment via snowfall, the firn air content (FAC) decreases, limiting its ability to take up future meltwater, a process known as firn air depletion. Firn air depletion is a known precursor to hydrofracture, and thus plays an important role in ice-shelf stability[17]. This work investigates future ice-shelf firn conditions over all Antarctic ice shelves, providing insight into which areas are vulnerable to firn air depletion and subsequent increased risk of hydrofracture in a warming climate.

For capturing the melt dynamics and the impact of meltwater percolation on firn structure, we use the complex, physics-based firn model SNOWPACK[18,19], which has been widely used in the polar regions[20–24]. SNOWPACK shows good agreement with observed FAC for a range of climatological conditions from Greenland[23], and has demonstrated a good agreement with microwave satellite observations on the number of days when meltwater is present on Antarctic ice shelves and with regional climate models on melt volumes[24]. We force SNOWPACK with historical and future-scenario meteorological output from the most recent

version of the Community Earth System Model[25] (CESM2) at 168 different ice-shelf sites (Figure 1a). Because ice lenses are known to impact the ability of surface meltwater to access deeper parts of the firn[17,26], we compute an effective FAC (FAC_e) from the SNOWPACK model output, by employing three slightly different ice lens thickness-permeability relationships (referred to as TP1, TP2, and TP3). These relationships account for the effect of ice lenses by reducing the storage space for meltwater below such lenses (ice lens thickness-permeability relationship TP1). We discuss results from the TP1 relationship, unless stated otherwise.

Complex firn models such as SNOWPACK are computationally expensive to run, thus limiting our ability to comprehensively assess future firn conditions and associated uncertainties under a range of climate forcings. Therefore, we use the SNOWPACK-calculated FAC_e to build a computationally simpler firn emulator, i.e. a fast, statistically-driven approximation of a more sophisticated model[27,28].

Our emulator was trained to estimate FAC_e using 10-year moving means of current and future ice-shelf climate conditions that are widely available Earth System Model (ESM) output (mean annual and summer air temperature, total annual precipitation, and mean annual wind speed). 10-year moving means of these climate variables were used to implicitly capture time dependence and to largely remove interannual variability and achieve a more representative mean climate. We first apply our emulator to estimate historical (1985–2015) ice-shelf FAC_e from ERA5 global reanalysis model output[29]. To predict 21st century change in FAC_e (ΔFAC_e), we run our emulator with changes in these climate variables from 35 different ESMs and 3 future Socio-economic Pathway (SSP) scenarios in the most recent Coupled Model Intercomparison Project[30] (CMIP6) added to the 'current-state' ERA5 climate (ERA5 + ΔESM). Our emulator allows for highly efficient ensembles of FAC_e predictions at large spatiotemporal scales using

readily available climate model output. Our emulator predicts that by 2100, Larsen C Ice Shelf is most at risk of firn air depletion, while Ross and Ronne-Filchner, which buttress more upstream ice, are likely to experience little ΔFAC_e. We further quantify uncertainties in our predictions of future ice-shelf firn air depletion and find that variability in ESM projections is the largest source of uncertainty, with the CMIP6-model range of ΔFAC_e predictions for a given SSP greater than the spread between SSP scenarios.

2 Results

2.1 Emulator Evaluation

After training on 80% of the data, our emulator demonstrates good performance on the remaining 20%. On this independent testing dataset, the emulator-predicted FAC_e explains 96% of the simulated SNOWPACK FAC_e variance, with a root mean squared error (RMSE) of 1.14 m and a mean bias of 14.8 mm (Figure 1c). Our emulator also generally does well at reproducing the total 21st century ΔFAC_e (Figure 1d) and the abrupt FAC_e changes observed in the SNOWPACK modelling (e.g. Figure 2a). However, because the emulator is trained using 10-year moving averages of climate variables and SNOWPACK FAC_e, it does not simulate FAC_e changes as abruptly as SNOWPACK at a given site. Supplementary Figure 1 shows that our emulator also reproduces 21st century firn air depletion at an ice-shelf and regional scale as well, compared to that simulated by SNOWPACK (Emulator vs. SNOWPACK ΔFAC_e r^2 = 0.97).

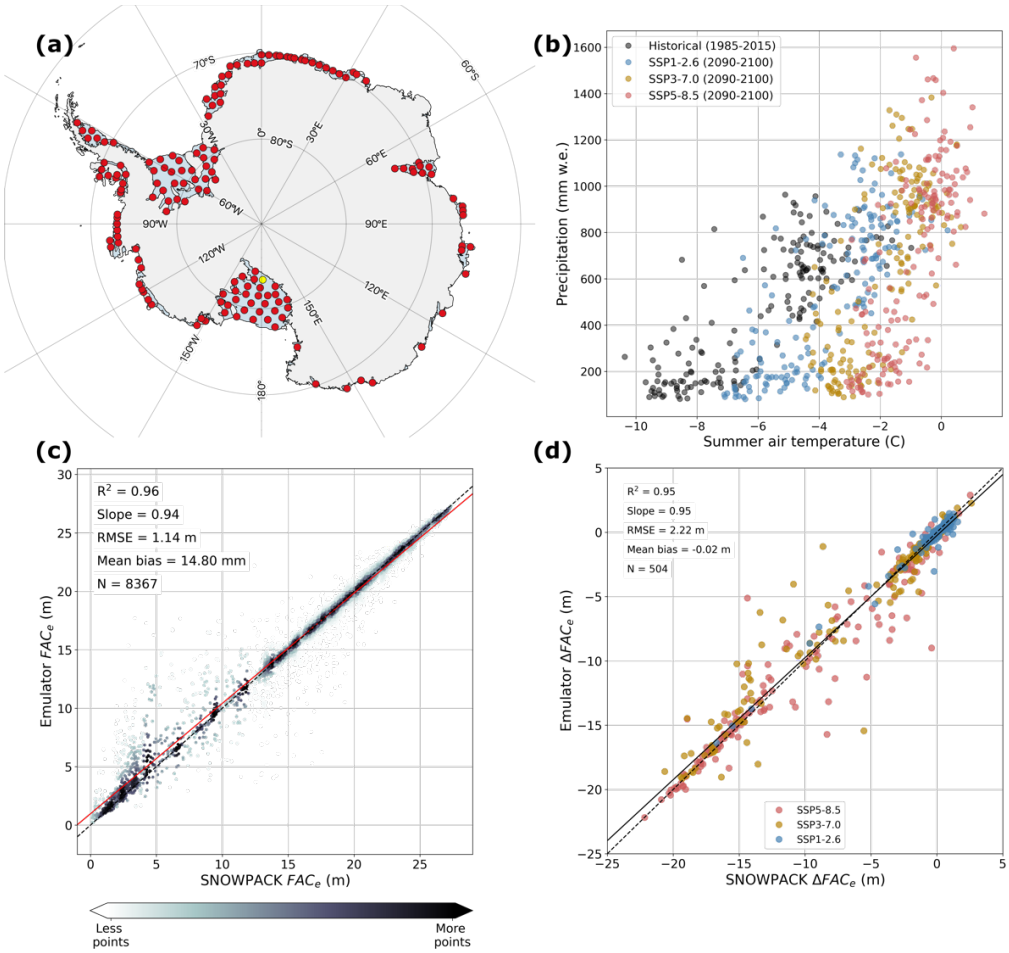

Figure 1: Evaluation of emulator performance vs. SNOWPACK at ice-shelf sites. **(a)** Map of 168 ice-shelf sites where the SNOWPACK model was forced with CESM2 historical and future output. The yellow dot represents the site featured in Figure 2. **(b)** Historical and future climate at each ice-shelf site. **(c)** SNOWPACK-predicted FAC_e vs. emulator-predicted FAC_e for our independent testing dataset (includes data from both historical and future scenarios). Points are colored according to point density within 2 m FAC_e segments along the x-axis, beginning at 0 m. The red line represents the line of best fit. **(d)** 21st century ΔFAC_e at each site from SNOWPACK and as predicted by our emulator, both forced with CESM2 climate output from the SSP1-2.6 (blue dots), SSP3-7.0 (golden dots), and SSP5-8.5 (red dots) future emission scenarios.

Out of the four variables used to train the emulator, the emulator finds that mean summer air temperature and total annual precipitation are the most important features for predicting ice-shelf FAC_e with relative feature importance scores of 0.442 and 0.327, respectively. These scores are determined based on the emulator training data and refer to how much the Gini Index for a feature decreases at each decision tree split, indicating the relative importance of the feature. Mean annual wind speed and air temperature have relative feature importance scores of 0.122

and 0.109, respectively. Summer air temperature influences FAC_e because it affects meltwater production in a strongly non-linear fashion[24,31]. Excessive surface meltwater refreezes in the firn to form ice lenses that impact vertical water percolation and severely deplete FAC[17,26]. Our emulator captures the impact of increasing ice lens thickness and concentration on FAC because it is trained on SNOWPACK FAC_e output that is adjusted considering overlying ice lenses (Section 2.2). With sufficient surface melt, thin ice layers can quickly merge to form thicker, impermeable ice slabs[32], a process we observe in our SNOWPACK output forced with the CESM2 SSP5-8.5 scenario (Figure 2). Counter-acting the firn air depletion is firn replenishment via snowfall [23,33], which makes up most of the annual precipitation over the AIS given the limited amount of rain in Antarctica.

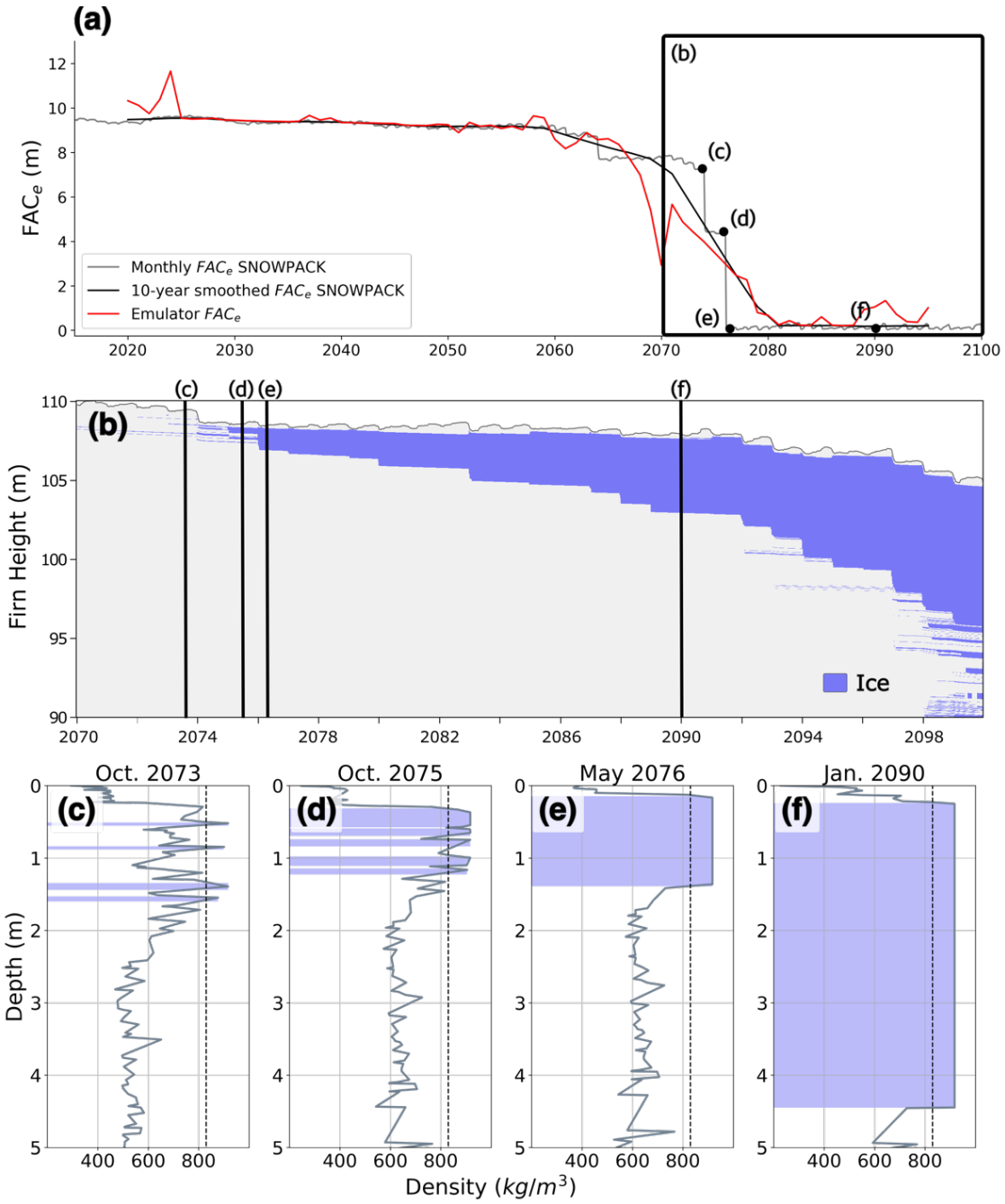

Figure 2: Example SNOWPACK model result of rapid ice lens development. **(a)** Timeseries of FAC_e from SNOWPACK forced with SSP5-8.5 CESM2 output. **(b)** Timeseries of ice layers. **(c-f)** Vertical density profiles at different timesteps. Layers > 830 kg m^{-3} (dashed black line) are considered to be ice lenses (blue). This site is on the Southern Ross Ice Shelf (178.75 °E, 83.403141 °S, Figure 1a). CESM2 simulates substantially warmer historical temperatures at this site compared with ERA5 (Supplementary Figure 2), hence warmer present day CESM2 air temperatures help promote future ice lens development under the SSP5-8.5 scenario.

2.2 21st century changes in FAC_e predicted by the emulator

To discuss predicted changes in FAC_e here, we focus on the CMIP6 model-median FAC_e. The CMIP6 model-spread for each ice shelf can be found in Figure 3 and Supplementary Table 1, and ice-shelf locations can be found in Supplementary Figure 3. Averaged during the historical period (1985–2015), individual ice-shelf FAC_e ranges from 9.4 ± 2.3 m for Scar Inlet to 25.5 ± 0.7 m for Venable, with a mean FAC_e for all Antarctic ice shelves ($\overline{FAC_e}$) of 16.3 ± 2.9 m (± 1 standard deviation across all ice shelves; Figure 4). In East Antarctica, areas of relatively lower FAC_e occur near the ice-shelf grounding line, coinciding with surface meltwater ponds observed by Ref. [34] (Supplementary Figure 4). By the end of the century (2090–2100), our emulator predicts no Antarctic-wide $\overline{\Delta FAC_e}$ under the SSP1-2.6 scenario ($\overline{FAC_e}$ of 16.3 ± 3.0 m) due to end-of-century summer air temperatures that have not warmed sufficiently for substantial meltwater production and ice lens formation to occur (Supplementary Figure 5a). For the SSP3-7.0 scenario, our emulator predicts a 0.7 ± 5.0 m (4%) decrease ($\overline{FAC_e}$ of 15.6 ± 4.0 m), and for the SSP5-8.5 scenario, a 1.3 ± 5.4 m (8%) decrease ($\overline{FAC_e}$ of 15.0 ± 4.6 m, Figure 4).

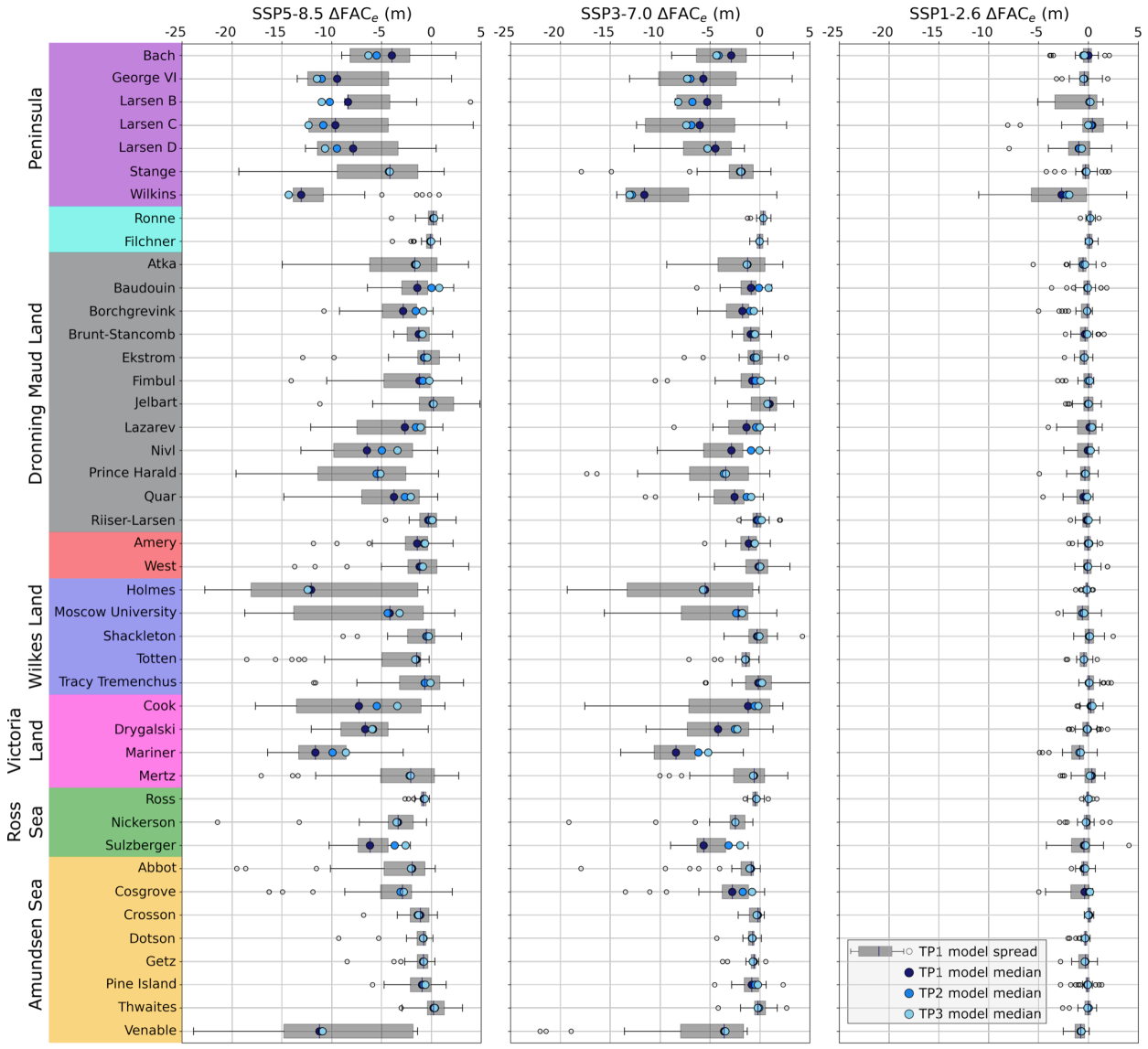

Figure 3: ΔFAC_e change from SSP5-8.5 (left), SSP3-7.0 (middle) and SSP1-2.6 (right) over individual ice shelves using different ice lens thickness-permeability relationships (TP1, TP2, TP3) and the CMIP6 model spread using TP1, equation (2) (Section 5.2). Ice shelves are grouped by region[35] (See Supplementary Figure 3 for ice-shelf regions).

Looking at ice shelves individually, for the low-emission SSP1-2.6 scenario, very little ΔFAC_e is predicted across most ice shelves. The only ice shelf projected to see > a 10% decrease in FAC_e is Wilkins, with ΔFAC_e = 2.7 m (an 18% decrease). However, Wilkins also has the largest CMIP6 model-spread in ΔFAC_e projections for this scenario (-11.0 to +3.2 m). A decline in FAC_e is more pronounced in the SSP3-7.0 scenario, where 18 of 43 ice shelves are projected

to experience > a 10% decrease in FAC_e. Further, using SSP3-7.0, there are 9 ice shelves where FAC_e decreases by > 25% and 2 that decrease by > 50% (Wilkins and Scar Inlet). While a FAC_e decline is found across nearly all ice shelves in this scenario (with the exception of Ronne and Jelbart), firn air depletion is predicted to be most pronounced in the Antarctic Peninsula (AP) (ΔFAC_e = -6.3 m, a 44% decrease), with Wilkins, again, projected to experience the largest FAC_e decrease (-11.6 m, or 76%).

In the high-emission SSP5-8.5 scenario, substantial firn air depletion is more widespread for ice shelves outside the AP than in lower emission scenarios. By 2100, the majority of ice shelves (22 of 43) are expected to experience a FAC_e decrease of > 10%, while 13 ice shelves experience > a 25% decrease, and 6 experience > a 50% decrease. At the end of the century, all AP ice shelves (except for Stange) have < 10 m FAC_e, and Scar Inlet, Wilkins, and Larsen C have the lowest FAC_e of all Antarctic ice shelves, with 1.0, 2.1, and 3.9 m, respectively. Outside the AP, three additional ice shelves are predicted to have < 10 m FAC_e by the end of the century: Mariner and Drygalski in Victoria Land with 5.7 and 6.7 m, respectively, and Nivlisen in Dronning Maud Land with 9.1 m. Additionally, Venable in the Amundsen Sea region and Holmes in Wilkes land are predicted to experience a substantial decrease in FAC_e (-11.2 and -12.1 m, respectively), although these ice shelves also have a relatively large CMIP6 model-spread in the SSP5-8.5 scenario (Figure 3).

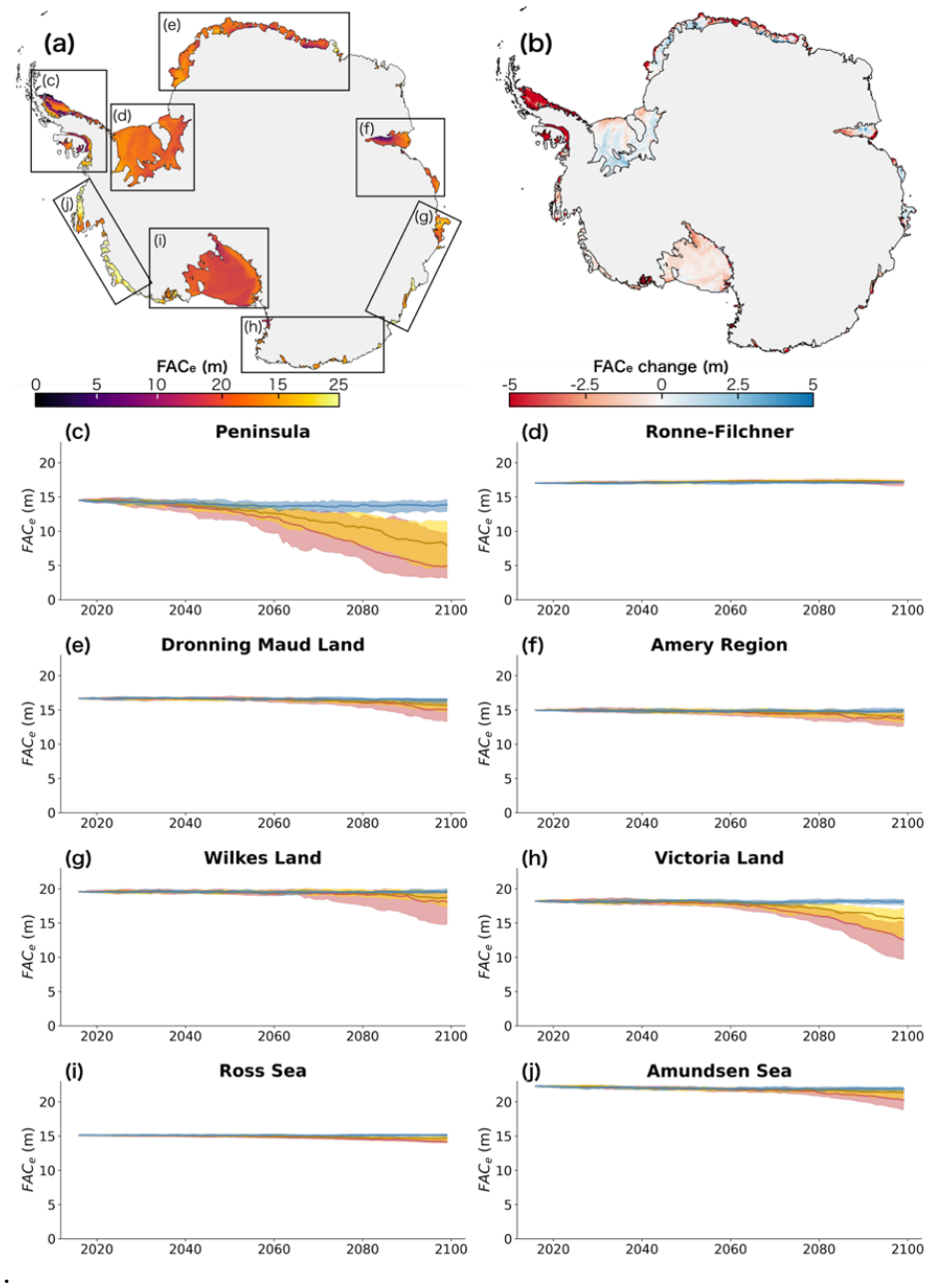

Figure 4: Historical AIS ice-shelf FAC_e and 21st century ΔFAC_e. **(a)** Present-day (1985–2015) FAC_e with boxed ice-shelf regions (See Supplementary Figure 3 for ice-shelf regions). **(b)** SSP5-8.5 end-of-century (2090–2100) ΔFAC_e. **(c-i)** Regional timeseries of 21st century FAC_e from each SSP scenario. The solid line represents the CMIP6 model-median and shading represents the 25th and 75th percentile range.

Antarctica's largest ice shelves, Ronne and Ross, are projected to experience minimal ΔFAC_e by 2100 under all emission scenarios and CMIP6 models (Figure 3,Figure *4*). Under SSP5-8.5, Ronne has a CMIP6 model-median FAC_e increase of 0.17 m (1%) while Ross has a

0.8 m (5.2%) decrease. Coincidentally, the Amundsen Sea region in West Antarctica, where the AIS is currently losing most of its mass, is also predicted to have relatively minimal ΔFAC_e, even in the high emission scenario. Under SSP5-8.5, ice shelves in this region are projected to lose 2.1 m FAC_e, and by 2100, Crosson, Dotson, and Getz have the highest FAC_e of all ice shelves (24.2, 23.9, and 23.2 m, respectively). Thwaites, where FAC_e increases by 0.2 m (1%), is also one of only three ice shelves in which our emulator predicts a FAC_e increase in the high emission scenario (the others being Ronne and Jelbart).

We find that 21st century ice-shelf ΔFAC_e is mostly driven by the absolute end-of-century summer air temperature, rather than the total change in summer air temperature. In fact, the ice shelves predicted to experience the largest SSP5-8.5 CMIP6 model-mean summer air temperature increase (Filchner: +4.1 °C, Ronne: +3.9 °C, and Ross: +3.8 °C), see minimal FAC_e decrease, as described above. In contrast, Bach, Scar Inlet and Wilkins, which are predicted experience some of the largest drops in FAC_e, correspondingly have the smallest predicted summer air temperature changes (+2.4 °C for all three). Instead, these three ice shelves have some of the highest summer air temperatures expected by 2100: 0.0 °C for Bach and 0.8 °C for both Larsen B and Wilkins.

2.3 Uncertainty in 21st century ΔFAC_e

Firn air content available for meltwater storage is impacted by the permeability of overlying ice lenses, which inhibit vertical water movement. A major assumption we make in this work is that ice lenses impact FAC_e related to their thickness by the relationship we introduced in equation (1) (TP1). However, testing two alternative approaches (TP2, TP3, see section 5.2) was found to yield similar ΔFAC_e on both a regional and ice-sheet-wide scale. For SSP5-8.5, FAC_e

across all ice shelves decreases by 1.3 m for both TP1 and TP2, and by 1.2 m using TP3. Regions that are too cold to produce consistent summer melt and thus have minimal ice lens formation, such as the Amundsen Sea, western Dronning Maud Land and the Ronne-Filchner and Ross regions, see minimal FAC_e decrease irrespective of the thickness-permeability relationship used (Figure 3). We find that the thickness-permeability relationship most substantially impacts FAC_e when ice lenses are relatively thin. For example, the average AP ice-shelf FAC_e during the historical period (1985–2015) changes by approximately 1 m depending on the thickness-permeability relationship used (14.2 m from TP1, 15.8 m from TP2, and 16.6 m from TP3). By 2100, when thicker ice slabs have formed across AP ice shelves in SSP5-8.5, the thickness-permeability relationship used becomes inconsequential (4.9 m FAC_e from TP1, 5.2 m from TP2, and 5.1 m from TP3). Limited field observations of ice lens permeability make modeling this process difficult and lead to unavoidable uncertainty regarding how ice lenses impact available FAC.

By far the largest source of uncertainty in future ΔFAC_e lies within CMIP6 climate model projections. For example, the 2090–2100 mean AIS-wide ice-shelf summer air temperature varies greatly across all CMIP6 models used in this study (-9.8 to -6.5 °C range in SSP1-2.6, -8.5 to -4.6 °C in SSP3-7.0, and -8.3 to -3.3 °C in SSP5-8.5). On the AP, end-of-century SSP5-8.5 CMIP6-modelled summer air temperature ranges from -2.2 to 3.7 °C, resulting in a wide range of estimated ΔFAC_e across the different CMIP6 models (-13.0 to +1.5 m). Similarly, Wilkes Land and Victoria Land have large ranges of predicted SSP5-8.5 ΔFAC_e (-11.3 to +2.4 m for Wilkes Land and -16.5 to +0.5 m for Victoria Land). In contrast, the narrower CMIP6 model-spread of predicted ΔFAC_e for Ronne-Filcher (-3.5 to +1.0 m) and Ross (-3.0 to +0.03 m)

suggest higher confidence that these larger ice shelves will not experience drastic firn air depletion by the end of this century.

The future emission scenario used presents another source of uncertainty, the impact of which is discussed throughout Section 2.2. However, we find that CMIP6 model uncertainty, which we define as the spread in CMIP6 model projections of 21st century ΔFAC_e, exceeds the range spanned by the emission scenarios. For example, for the AP region, where firn air depletion is expected to be the most drastic, the CMIP6-model-median ΔFAC_e ranges from -0.65 m for SSP1-2.6 to -9.6 for SSP5-8.5, a 8.95 m spread. In comparison, the CMIP6 model range of ΔFAC_e for SSP1-2.6, SSP3-7.0, and SSP5-8.5 is 8.9, 13.4, and 14.5 m, respectively, indicating that the CMIP6 model spread, and thus uncertainty, for SSP1-2.6 is comparable to the uncertainty across all scenarios, and for SSP3-7.0 and SSP5-8.5 is larger than the uncertainty across scenarios.

3 Discussion

Our emulator was trained using output from the SNOWPACK firn model; thus, any biases present in SNOWPACK will be inherited by our emulator. Because SNOWPACK is physics-based and therefore not tuned by or biased toward observational data, it may more realistically simulate firn properties under future climate conditions that are not captured in existing observations, compared with empirical models such as the Community Firn Model (CFM)[23]. On Antarctic ice shelves, SNOWPACK has demonstrated a good ability to reproduce melt days and melt day variability compared with satellite microwave observations, and melt volumes compared with RACMO2.3p2 and MARv3.12[24]. For the Greenland Ice Sheet, SNOWPACK was found to reproduce the observed spread in FAC across the ice sheet over a

range of climate conditions with variable amounts of melt[23]. Additionally, SNOWPACK accurately models the location of near-surface ice slabs compared with those detected in Operation Icebridge radar data[32,36]. However, firn physics are not fully understood and knowledge gaps in firn hydrological processes limit the ability of firn models to accurately simulate processes such as vertical meltwater percolation and lateral flow. More detailed observations of hydrologic firn processes are necessary to advance the development of firn models.

We find that more than 90% of all ice-shelf grid cells with mean summer air temperatures above 0 °C for any year have depleted FAC, which we define as less than 5 m FAC_e (Figure 5b). However, this summer air temperature threshold for firn air depletion appears to be lower for ice shelves that receive less precipitation (Figure 5a), indicating that dry ice shelves may be more vulnerable to surface meltwater-induced collapse if they undergo substantial warming. This specific finding agrees with the conclusion of Ref. [37]. While their work was done at a higher horizontal resolution than this study, their method used a fixed threshold for melt over accumulation ratio to assess firn air depletion. This fixed threshold assumes prescribed and invariable firn properties over the ice shelves[38], while our use of a physics-based, detailed firn model could be expected to better capture firn properties and melt dynamics in the firn layer in a changing climate.[39].

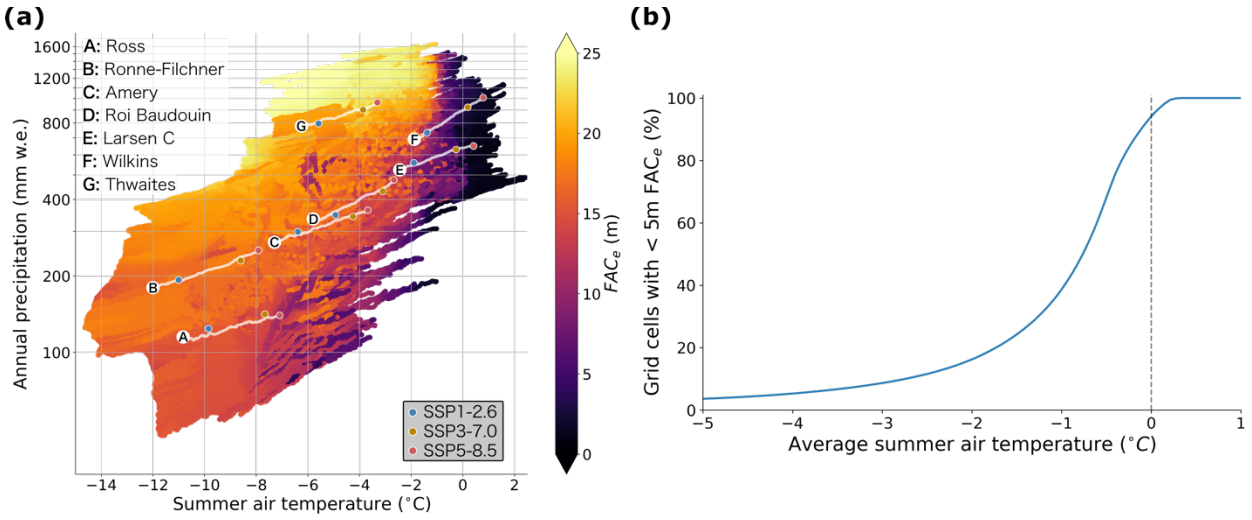

Figure 5: (a) Relationship between mean summer air temperature, total annual precipitation, and FAC_e. Data is from each ice-shelf grid cell below 1500 m for every year from 2015 to 2100 in the SSP3-7.0 and SSP5-8.5 scenarios. White lines represent the SSP5-8.5 projected path for seven ice shelves (A-G) with the 2090–2100 mean-state marked for SSP1-2.6 (blue dot), SSP3-7.0 (yellow dot) and SSP5-8.5 (red dot). **(b)** From (a), the percentage of ice-shelf grid cells with depleted firn (< 5 m FAC_e) for mean summer air temperatures ranging from -5 to 1 °C.

While colder and dryer ice shelves may be more vulnerable to surface-melt-induced collapse at colder air temperatures than the warmer and wetter ice shelves, it is unlikely, even in the high-emission scenario, that these ice shelves will experience enough warming throughout the 21st century for substantial firn air depletion to occur. According to ERA5, the current (1985–2015) mean summer air temperature for Ronne-Filchner and Ross is -11.8 and -10.7 °C, respectively, indicating that these ice shelves would need to warm substantially to experience surface meltwater ponding. In contrast, to reach a mean summer air temperature of 0 °C, the AP Wilkins and Larsen C ice shelves need to warm only by 1.6 and 2.2 °C, respectively, a likely occurrence in most CMIP6 SSP5-8.5 and many CMIP6 SSP3-7.0 models. Areas of high, localized annual melt due to persistent warm foehn or katabatic winds (e.g. portions of the Amery or Roi Baudouin ice shelves[40,41] are too small to be captured by ERA5 and the ESMs in this work. Because of this, our emulator may overestimate FAC_e in these areas of high localized

melt, implying that these areas may be more vulnerable to firn air depletion than our emulator estimates.

Several factors contribute to ice-shelf vulnerability, including accumulation, surface and basal melt rates and stress regimes. Ref. [35] provides ice-shelf vulnerability indexes based on an observed relationship between annual melt days and scatterometry backscatter. Similar to what we find here, they show that AP ice shelves are the most vulnerable to surface-melt-induced firn air depletion and potential collapse, and that Ronne-Filchner and Ross are least vulnerable. However, not all ice shelves that we find are likely to experience substantial firn air depletion are susceptible to hydrofracturing and break-up. For example, Ref. [42] maps ice-shelf areas where tensile stresses may promote hydrofracturing. They show that several AP ice shelves which we predict to have substantial firn air depletion such as Wilkins, Bach and George VI, have low tensile resistive stresses (including compressive stresses for George VI[43]), making them more resilient to hydrofracture, despite the fact that these three ice shelves usually experience widespread meltwater ponding each summer[44]. Additionally, ice shelves in Victoria Land, such as Mariner and Drygalski, which we project will experience substantial firn air depletion in the high-emission scenario, do not buffer substantial inland ice[42], and thus would be less impactful than many other ice shelves if they were to break-up. We conclude that Larsen C is the most vulnerable ice shelf to a surface-melt-induced collapse event this century due to its high likelihood of depleted FAC_e and sufficiently high tensile stresses for fracture[42]. Further, if Larsen C does break-up, a large volume of upstream ice would be impacted because of its higher buttressing capacity compared to other ice shelves projected to experience similar firn air depletion.

4 Conclusions

Ice-shelf firn is important for ice-shelf stability by storing meltwater that may otherwise pond on the surface and impact ice-shelf stability. Here, we run the physics-based firn model, SNOWPACK, forced with CESM2 historical and future model output over ice shelves. We calculate an effective FAC (FAC_e) that accounts for the impact of ice lenses on subsurface meltwater percolation. Using SNOWPACK-calculated FAC_e, we develop a computationally less expensive emulator that uses a random forest to predict ice-shelf FAC_e based on climate conditions. We use our emulator to estimate future ΔFAC_e from multiple future scenarios, a suite of CMIP6 models, and across all Antarctic ice shelves — a problem that would be computationally impractical using a traditional firn model.

We find that mean absolute summer air temperature is the most important indicator for changes in ice-shelf FAC, suggesting that firn models require an accurate representation of this variable as input. According to SSP1-2.6, 21st century ice-shelf ΔFAC_e is minimal across the AIS. Under high emission scenarios SSP3-7.0 and SSP5-8.5, we find that the Larsen C Ice Shelf is most at risk of firn air depletion by 2100, while ice shelves that buttress more upstream ice, such as Ross and Ronne-Filchner, are likely to see little FAC change. The largest source of uncertainty regarding future ice-shelf FAC comes from CMIP6 model predictions of temperature change throughout the 21st century because the models have varying climate sensitivity to increased greenhouse gases. For most ice shelves, it is in fact uncertain if substantial firn air depletion can be expected by 2100, except for the low emission SSP1-2.6 scenario, for which models agree that the majority of ice shelves will experience little change in FAC.

5 Methods

5.1 Firn modeling

The goal of our firn emulator is to replace a more sophisticated, computationally expensive firn model to make FAC predictions into the future under a range of climatological conditions. Our firn emulator was built to mimic how the detailed, physics-based, multi-layer model SNOWPACK[18,19] simulates FAC under these different climatological conditions. SNOWPACK has previously been modified for use on ice sheets[20,21,36,45] and ice shelves[22,24], showing good performance at reproducing FAC over the Greenland Ice Sheet for a range of climate conditions[23] and good comparison of Antarctic ice shelf melt days with microwave satellite observations and melt volume with regional climate models[24]. We forced SNOWPACK with historical and future CESM2 output[25,39], providing a consistent forcing over this wide range of potential climates. It is critical that firn simulations from potential future climates were included in the emulator training dataset because the historical period exhibits substantially less melt than predicted for the future and we wanted our emulator to make future FAC predictions as well.

Using the MEaSUREs v2 Antarctic Boundaries ice shelves map[46,47], we selected 168 CESM2 ice-shelf grid cells that are representative of a variety of different ice-shelf climates (Figure 1b). For each grid cell, we extracted 3-hourly air temperature, relative humidity and incoming shortwave radiation, and daily wind speed, incoming longwave radiation and precipitation output from CESM2 historical (1850–2015) and future (2015–2100) Shared Socio-economic Pathway (SSP) SSP1-2.6, SSP3-7.0 and SSP5-8.5 simulations[48].

SNOWPACK was spun-up over the period 1850–1900 for as many repeats as necessary to build up a 100 m column of snow, firn, and ice. We then ran the final simulation from 1850–2015 for the historical scenario and 2015–2100 for each SSP scenario. Model settings were similar as described in Ref. [20], except for the treatment of the lower boundary for solving the heat equation for which we followed Ref. [24] by prescribing a fixed lower-boundary temperature of -1.8 °C: the freezing point of ocean water.

5.2 Determination of effective FAC

SNOWPACK provides, among other output, the volumetric air content (θ_a, $m^3\ m^{-3}$) in each vertical layer i. We computed effective FAC (in meters) over the N layers constituting the full firn column using:

$$FAC_e = \sum_{i=1}^{N} f(i)\ \theta_a(i)\ \Delta z(i)$$

Equation (1)

where $\Delta z(i)$ is the layer thickness (in meters) of layer i and $f(i)$ is a weight applied to $\theta_a(i)$ for each layer. The default definition of FAC is congruent with $f(i) = 1$. By varying $f(i)$, we introduce and effective FAC (FAC_e) to account for the presence of ice lenses, which inhibit meltwater from reaching the pore space below. Here, we define ice layers as having a density > 830 kg m^{-3} (the pore close-off density[49]). Weights $f(i)$ are determined based on work by Ref. [50], in which the authors scale hydraulic conductivity in Darcy's law to account for the effect of ice lenses. Based on evidence of relatively unobstructed meltwater penetration through ice layers up to 0.12 m thick at DYE-2, Greenland[51], we assumed ice layers < 0.1 m are fully permeable and thus all pore space below these small ice layers is included in our calculation of FAC_e (i.e.,

$f(i) = 1$). Following Ref. [50], we also assumed that ice layers > 0.5 m thick are impermeable to meltwater (i.e., $f(i) = 0$), meaning that firn below these thick ice layers is excluded from our FAC_e calculation. Given M ice layers above layer i, for each ice layer j above layer i with thickness t_j between 0.1 and 0.5 m, we prescribed a nonlinear decrease in FAC_e below these ice layers:

$$f(i) = \sum_{j=1}^{M} A^{-\gamma(t_j - 0.1)}$$

Equation (2)

with $A = 10$ and $\gamma = 10$[50]. Weights $f(i)$ are limited between 0 and 1. We refer to this ice lens thickness-permeability relationship as TP1 (Supplementary Figure 6).

To test the sensitivity of our results to this assumed relationship, we implement two other ice lens thickness-permeability relationships. The first alternate relationship follows equation (2) with $A = 4$ and $\gamma = 4$, providing a less aggressive decrease in permeability with thickness (we will refer to this relationship as TP2). The other relationship we consider is also a variant of equation (2), applying a linear decrease in permeability with ice lens thickness from 0.1 to 1 m (referred to as TP3):

$$f(i) = \sum_{j=1}^{M} 1 - \frac{t_j - 0.1}{0.9}$$

Equation (3)

For both alternate relationships TP2 and TP3, we assume that ice lenses > 1 m are fully impermeable and maintain the assumption that ice lenses < 0.1 m are fully permeable[50,51] (Supplementary Figure 6).

5.3 FAC Emulator

Using FAC_e from the SNOWPACK model output, we built an emulator which allows us to efficiently estimate FAC_e across all Antarctic ice shelves for numerous climate model scenarios. The climate variables used as FAC_e predictors were: total annual precipitation, mean annual 10 m wind speed, mean annual 2 m air temperature and mean austral summer (DJF) 2 m air temperature. These climate variables are 1) known to impact surface firn density, compaction rate and meltwater production, all which impact FAC_e, and 2) readily available from most CMIP6 climate models. We computed 10-year moving averages of these variables to largely remove interannual variability and achieve a more representative mean climate, at the expense of capturing inter-annual variability. As a result, our input dataset consisted of 21-timesteps of 10-year moving means from the historical period (1990–2010) and 76-timesteps of 10-year moving means from future emission scenarios SSP1-2.6, SSP3-7.0 and SSP5-8.5 (2020–2095) at each of the 168 ice-shelf sites for which we employed SNOWPACK. In total, our input dataset consisted of 41,832 entries (168 sites * (21 historical years + 76 future years * 3 scenarios)), which we divided into two groups such that 80% was used for model training and 20% was used for testing. Our predicted variable was the 10-year moving average of mean October FAC_e (just before the melt season onset) at corresponding timesteps and locations. To maximize the points used for training, the emulator does not consider dependence in FAC_e between successive years. This dependence, however, is implicitly captured through the 10-year moving averaged inputs. Additionally, we only consider total precipitation and not precipitation type because 1) precipitation partitioned into solid and liquid precipitation is less common GCM output, and 2) our emulator was shown to have a low FAC_e bias at sites with higher summer air temperatures

(Figure 1c), indicating that neglecting to account for temporal changes in the rain/snow ratio has not led to a substantial source of error.

Our emulator was built using a random forest (RF) model, which we trained and implemented using the Python sci-kit learn library[52]. Our RF was comprised of 100 decision trees, each optimized on a bootstrapped sample of the training dataset. The hyperparameters used for our RF model are listed below (*points in italics* indicate parameters that differ from the scikit-learn default):

- Number of trees `('n_estimators') = 100`
- Cost function `('criterion') = L2 loss ('squared_error')`
- Maximum tree depth `('max_depth') = None`
- Minimum samples required to split a node `('min_samples_split') = 2`
- Minimum leaf size = `'min_samples_leaf' = 1`
- Number of features to consider when looking for the best split `('max_features') = 'auto'`
- `'bootstrap' = True`
- *Use out-of-bag samples to estimate the generalization score `('oob_score') = True`*
- Number of samples to draw from X to train each base estimator `('max_samples') = None`

To test our RF hyperparameter choice we randomly selected 100 different combinations of the following scikit-learn hyperparameters:

- `'max_depth' = [5, 10, 25, 50, 100, None]`
- `'max_features' = ['auto', 'sqrt']`
- `'min_samples_leaf' = [1, 2, 4]`
- `'min_samples_split' = [2, 5, 10]`
- `'n_estimators' = [10, 50, 100, 200]`

The optimal hyperparameters from this randomized search were: `'max_depth' = None, 'max_features' = 'sqrt', 'min_samples_leaf' = 1,`

`'min_samples_split' = 2, 'n_estimators' = 200` (where *italics* indicates hyperparameters that differ from scikit-learn default values). We then compared this optimal model from our randomized search with the default hyperparameters and found that the default model had a marginally better mean 5-fold cross validation score (0.9526 ± 0.0033 for the default model and 0.9522 ± 0.0031). As such, we chose to use the default scikit-learn hyperparameters for our random forest (except for `'oob_score' = True`).

5.4 Current and Future FAC_e

We estimated present-day ice-shelf FAC_e by running our firn emulator with input data from the ECMWF ERA5 reanalysis dataset[29]. We used ERA5 because it has the smallest near-surface temperature bias relative to the observations and best represents accumulation[53,54].

To predict ice-shelf FAC_e throughout the 21st century, we used changes in mean annual near-surface air temperature, summer air temperature, wind speed, and total annual precipitation from CMIP6 models[30] (Supplementary Table 2). From the 88 available CMIP6 models, we only used the 34 models with temperature, wind speed, and precipitation output available on the Pangeo platform from the historical period and future SSP1-2.6, SSP3-7.0, and SSP5-8.5 scenarios. To map a future FAC_e envelope, we used the low-emission (SSP1-2.6) and high-emission (SSP5-8.5) scenarios, and included SSP3-7.0 as a more likely high-end emission scenario[55]. CMIP6 model output was regridded using bilinear interpolation to the ERA5 grid. Changes in these climate variables were added to the 'current-state' climate from ERA5 to remove possible bias in the CMIP6 models representation of the current climate ('delta-change' method[56,57]). We again computed 10-year moving averages (from 2020–2095) of these climate variables as input for the emulator.

We only considered ice shelves with > 5 ERA5 grid cells with a modelled elevation <1500 m above sea level, resulting in 43 ice shelves, which we divided into 8 regions[35] for a comparison of regional ΔFAC_e (Supplementary Figure 3). To determine the 21st centuryΔFAC_e, we subtract the mean historical (1985–2015) FAC_e from the 2095 value, which represents an end-of-century mean-state FAC_e, because our emulator input is 10-year moving averages of climate variables. We calculate % change in FAC_e with respect to the total ice-shelf FAC_e, not for each grid cell.

Additionally, we ensured that the dataset used for training covers the range of climatic conditions used in these emulator simulations. We compared climate conditions used for training (raw-CESM2 output) with conditions used in the emulator simulations (ERA5 + ΔGCM mean). Supplementary Figure 5b shows that the emulator simulations do not extrapolate greatly beyond the data used for training. In cases where extrapolation does occur (e.g. the Ronne ice shelf where ERA5 historical conditions are colder than the training dataset), FAC_e change will be minimal and the emulator performs as expected given these colder conditions. Further, the firn air depletion transition is well represented in the training data and thus the training data set is appropriate for how we implement the emulator.

Open Science

Code availability

The SNOWPACK model code is available at: https://github.com/snowpack-model/snowpack. Code used for the analysis in the project is published at https://doi.org/10.5281/zenodo.7574637.

Data availability

ERA5 reanalysis output can be downloaded at https://doi.org/10.24381/cds.adbb2d47. Input and FAC results from the SNOWPACK model can be found at https://doi.org/10.5281/zenodo.7535507. The emulator models and emulator FAC results can be found at https://doi.org/10.5281/zenodo.7535208. Instructions and examples for how to access CMIP6 model output from the Pangeo Platform can be found at https://gallery.pangeo.io/repos/pangeo-gallery/cmip6/.

Acknowledgments

D.D. was supported by NASA FINESST Fellowship #80NSSC19K1329 and by the iHARP HDR Institute (NSF award #2118285). A.F.B. received support from the NSF under award #1841607 to the University of Colorado Boulder. N.W. was supported by NASA IDS grant #80NSSC20K1727. We acknowledge high-performance computing support from Cheyenne (doi:10.5065/D6RX99HX) provided by NCAR's Computational and Information Systems Laboratory, sponsored by the NSF. This work also utilized the Summit supercomputer, which is supported by the NSF (awards ACI-1532235 and ACI-1532236) and is a joint effort of the University of Colorado Boulder, and Colorado State University. Data storage supported by the University of Colorado Boulder 'PetaLibrary'.

References

1. Rignot, E. *et al.* Four decades of Antarctic ice sheet mass balance from 1979–2017. *Proceedings of the National Academy of Sciences of the United States of America* Preprint at https://doi.org/10.1073/pnas.1812883116 (2019).
2. Pattyn, F. *et al.* The Greenland and Antarctic ice sheets under 1.5 °C global warming. *Nat Clim Chang* **8**, 1053–1061 (2018).
3. Dupont, T. K. & Alley, R. B. Assessment of the importance of ice-shelf buttressing to ice-sheet flow. *Geophys Res Lett* **32**, 1–4 (2005).
4. Fürst, J. J. *et al.* The safety band of Antarctic ice shelves. *Nat Clim Chang* **6**, 479–482 (2016).
5. Rignot, E. *et al.* Accelerated ice discharge from the Antarctic Peninsula following the collapse of Larsen B ice shelf. *Geophys Res Lett* **31**, 2–5 (2004).
6. De Angelis, H. & Skvarca, P. Glacier surge after ice shelf collapse. *Science (1979)* **299**, 1560–1562 (2003).
7. Pritchard, H. D. *et al.* Antarctic ice-sheet loss driven by basal melting of ice shelves. *Nature* **484**, 502–505 (2012).
8. Smith, B. *et al.* Pervasive ice sheet mass loss reflects competing ocean and atmosphere processes. *Science (1979)* **368**, 1239–1242 (2020).
9. van den Broeke, M. Strong surface melting preceded collapse of Antarctic Peninsula ice shelf. *Geophys Res Lett* **32**, n/a-n/a (2005).
10. Scambos, T. A., Hulbe, C., Fahnestock, M. & Bohlander, J. The link between climate warming and break-up of ice shelves in the Antarctic Peninsula. *Journal of Glaciology* (2000) doi:10.3189/172756500781833043.
11. Holland, P. R. *et al.* Oceanic and atmospheric forcing of Larsen C Ice-Shelf thinning. *Cryosphere* **9**, 1005–1024 (2015).
12. Banwell, A. F., MacAyeal, D. R. & Sergienko, O. V. Breakup of the Larsen B Ice Shelf triggered by chain reaction drainage of supraglacial lakes. *Geophys Res Lett* (2013) doi:10.1002/2013GL057694.
13. Robel, A. A. & Banwell, A. F. A Speed Limit on Ice Shelf Collapse Through Hydrofracture. *Geophys Res Lett* **46**, 12092–12100 (2019).
14. Leeson, A. A., Forster, E., Rice, A., Gourmelen, N. & van Wessem, J. M. Evolution of Supraglacial Lakes on the Larsen B Ice Shelf in the Decades Before it Collapsed. *Geophys Res Lett* (2020) doi:10.1029/2019GL085591.
15. Scambos, T. A. *et al.* Ice shelf disintegration by plate bending and hydro-fracture: Satellite observations and model results of the 2008 Wilkins ice shelf break-ups. *Earth Planet Sci Lett* (2009) doi:10.1016/j.epsl.2008.12.027.
16. Pattyn, F. & Morlighem, M. The uncertain future of the Antarctic Ice Sheet. *Science (1979)* **367**, 1331–1335 (2020).
17. Munneke, P. K., Ligtenberg, S. R. M., Van Den Broeke, M. R. & Vaughan, D. G. Firn air depletion as a precursor of Antarctic ice-shelf collapse. *Journal of Glaciology* (2014) doi:10.3189/2014JoG13J183.

18. Bartelt, P. & Lehning, M. A physical SNOWPACK model for the Swiss avalanche warning Part I: Numerical model. *Cold Reg Sci Technol* (2002) doi:10.1016/S0165-232X(02)00074-5.
19. Lehning, M., Bartelt, P., Brown, B., Fierz, C. & Satyawali, P. A physical SNOWPACK model for the Swiss avalanche warning Part II. Snow microstructure. *Cold Reg Sci Technol* (2002) doi:10.1016/S0165-232X(02)00073-3.
20. Keenan, E. *et al.* Physics-based SNOWPACK model improves representation of near-surface Antarctic snow and firn density. *Cryosphere* (2021) doi:10.5194/tc-15-1065-2021.
21. Dunmire, D. *et al.* Observations of buried lake drainage on the Antarctic Ice Sheet. *Geophys Res Lett* **47**, e2020GL087970 (2020).
22. Alley, K. E. *et al.* Two decades of dynamic change and progressive destabilization on the Thwaites Eastern Ice Shelf. *Cryosphere* **15**, 5187–5203 (2021).
23. Thompson-Munson, M., Wever, N., Stevens, C. M., Lenaerts, J. T. M. & Medley, B. An evaluation of a physics-based firn model and a semi-empirical firn model across the Greenland Ice Sheet (1980–2020). *Cryosphere* **17**, 2185–2209 (2023).
24. Banwell, A. F., Wever, N., Dunmire, D. & Picard, G. Quantifying Antarctic-Wide Ice-Shelf Surface Melt Volume Using Microwave and Firn Model Data: 1980 to 2021. *Geophys Res Lett* **50**, (2023).
25. Danabasoglu, G. *et al.* The Community Earth System Model Version 2 (CESM2). *J Adv Model Earth Syst* **12**, 1–35 (2020).
26. Machguth, H. *et al.* Greenland meltwater storage in firn limited by near-surface ice formation. *Nat Clim Chang* (2016) doi:10.1038/nclimate2899.
27. O'Hagan, A. Bayesian analysis of computer code outputs: A tutorial. *Reliab Eng Syst Saf* **91**, 1290–1300 (2006).
28. Verjans, V. *et al.* Uncertainty in East Antarctic Firn Thickness Constrained Using a Model Ensemble Approach. *Geophys Res Lett* **48**, 1–11 (2021).
29. Hersbach, H. *et al.* The ERA5 global reanalysis. *Quarterly Journal of the Royal Meteorological Society* **146**, 1999–2049 (2020).
30. Eyring, V. *et al.* Overview of the Coupled Model Intercomparison Project Phase 6 (CMIP6) experimental design and organization. *Geosci Model Dev* **9**, 1937–1958 (2016).
31. Trusel, L. D. *et al.* Divergent trajectories of Antarctic surface melt under two twenty-first-century climate scenarios. *Nature Geoscience* Preprint at https://doi.org/10.1038/ngeo2563 (2015).
32. MacFerrin, M. *et al.* Rapid expansion of Greenland's low-permeability ice slabs. *Nature* **573**, 403–407 (2019).
33. Rennermalm, Å. K. *et al.* Shallow firn cores 1989–2019 in southwest Greenland's percolation zone reveal decreasing density and ice layer thickness after 2012. *Journal of Glaciology* **68**, 431–442 (2022).
34. Stokes, C. R., Sanderson, J. E., Miles, B. W. J., Jamieson, S. S. R. & Leeson, A. A. Widespread distribution of supraglacial lakes around the margin of the East Antarctic Ice Sheet. *Sci Rep* **9**, 1–14 (2019).
35. Alley, K. E., Scambos, T. A., Miller, J. Z., Long, D. G. & MacFerrin, M. Quantifying vulnerability of Antarctic ice shelves to hydrofracture using microwave scattering properties. *Remote Sens Environ* **210**, 297–306 (2018).

36. Thompson{-}Munson, M., Wever, N., Stevens, M. C., Lenaerts, J. T. M. & Medley, B. Observed and modeled Greenland firn properties (1980–2020). *The Cryosphere Discussions* (2022) doi:https://doi.org/10.5194/tc-2022-223.
37. van Wessem, J. M., van den Broeke, M. R., Wouters, B. & Lhermitte, S. Variable temperature thresholds of melt pond formation on Antarctic ice shelves. *Nat Clim Chang* **13**, 161–166 (2023).
38. Donat-Magnin, M. *et al.* Future surface mass balance and surface melt in the Amundsen sector of the West Antarctic Ice Sheet. *Cryosphere* **15**, 571–593 (2021).
39. Dunmire, D., Lenaerts, J. T. M., Datta, R. T. & Gorte, T. Antarctic surface climate and surface mass balance in the Community Earth System Model version 2 during the satellite era and into the future (1979–2100). *Cryosphere* **16**, 4163–4184 (2022).
40. Zwally, H. J. & Fiegles, S. Extent and duration of Antarctic surface melting. *Journal of Glaciology* **40**, 463–476 (1994).
41. Lenaerts, J. T. M. *et al.* Meltwater produced by wind-albedo interaction stored in an East Antarctic ice shelf. *Nat Clim Chang* (2017) doi:10.1038/nclimate3180.
42. Lai, C. Y. *et al.* Vulnerability of Antarctica's ice shelves to meltwater-driven fracture. *Nature* **584**, 574–578 (2020).
43. Labarbera, C. H. & Macayeal, D. R. Traveling supraglacial lakes on George VI Ice Shelf , Antarctica. **38**, 1–5 (2011).
44. Banwell, A. F. *et al.* The 32-year record-high surface melt in 2019/2020 on the northern George VI Ice Shelf, Antarctic Peninsula. *Cryosphere* **15**, 909–925 (2021).
45. Dunmire, D., Banwell, A., Lenaerts, J. & Datta, R. T. Contrasting regional variability of buried meltwater extent over two years across the Greenland Ice Sheet. *The Cryosphere Discussions* (2021) doi:10.5194/tc-2021-3.
46. Mouginot, J., Scheuchl, B. & Rignot, E. MEaSUREs Antarctic Boundaries for IPY 2007-2009 from Satellite Radar, Version 2. Preprint at https://doi.org/https://doi.org/10.5067/AXE4121732AD (2017).
47. Rignot, E., Mouginot, J. & Scheuchl, B. MEaSUREs Antarctic Grounding Line from Differential Satellite Radar Interferometry, Version 2. *NASA National Snow and Ice Data Center Distributed Active Archive Center* (2016) doi:https://doi.org/10.5067/IKBWW4RYHF1Q.
48. Meinshausen, M. *et al.* The shared socio-economic pathway (SSP) greenhouse gas concentrations and their extensions to 2500. *Geosci Model Dev* **13**, 3571–3605 (2020).
49. Martinerie, P., Raynaud, D., Etheridge, D. M., Barnola, J.-M. & Mazaudier, D. Physical and climatic parameters which influence the air content in polar ice. *Earth Planet Sci Lett* **112**, 1–13 (1992).
50. Samimi, S., Marshall, S. J., Vandecrux, B. & MacFerrin, M. Time-Domain Reflectometry Measurements and Modeling of Firn Meltwater Infiltration at DYE-2, Greenland. *J Geophys Res Earth Surf* **126**, (2021).
51. Samimi, S., Marshall, S. J. & MacFerrin, M. Meltwater Penetration Through Temperate Ice Layers in the Percolation Zone at DYE-2, Greenland Ice Sheet. *Geophys Res Lett* **47**, 1–9 (2020).
52. Pedregosa, F. *et al.* Scikit-learn: Machine Learning in Python. *Journal of Machine Learning Research* **12**, 2825–2830 (2011).

53. Gossart, A. *et al.* An evaluation of surface climatology in state-of-the-art reanalyses over the Antarctic Ice Sheet. *J Clim* **32**, 6899–6915 (2019).
54. Zhu, J. *et al.* An Assessment of ERA5 Reanalysis for Antarctic Near-Surface Air Temperature. *Atmosphere (Basel)* **12**, (2021).
55. IPCC. *IPCC, 2021: Climate Change 2021: The Physical Science Basis. Contribution of Working Group I to the Sixth Assessment Report of the Intergovernmental Panel on Climate Change*. (2021).
56. Rummukainen, M. State-of-the-art with regional climate models. *Climate Change* **1**, 82–96 (2010).
57. Maraun, D. Bias Correcting Climate Change Simulations - a Critical Review. *Curr Clim Change Rep* **2**, 211–220 (2016).